LONG AND INTERMEDIATE WAVELENGTH FLAW RECONSTRUCTION

D. O. Thompson and S. J. Wormley

Ames Laboratory, USDOE
Iowa State University
Ames, IA 50011

ABSTRACT

An automated multiviewing ultrasonic transducer and a first generation signal processing program have been developed for the purpose of detecting and characterizing flaws in materials. The multiviewing transducer has been designed and developed to exploit advances in theoretical inverse elastic wave scattering in the long and intermediate wavelength regime made in recent years. The signal processing algorithm has been assembled as a first step in the development of a decision-tree algorithm for flaw characterization. First results that have been obtained in a completely automatic mode are given in this paper. It is concluded that this new long and intermediate wavelength, model-based reconstruction is feasible and potentially very useful in quantitative NDE applications on real systems.

INTRODUCTION

Because of the potential for the characterization of flaws that results from the theoretical base for inverse scattering in the long and intermediate wavelength regimes established in recent years (1,2,3, 4,5,6,7) and because of the importance of this regime to practical inspection technology, this project was initiated approximately three years ago. Its purposes were twofold: 1) to design and develop instrumentation that would serve to implement the theoretical inverse flaw characterization capabilities, and 2) to pursue the development of a decision-tree logic for flaw characterization through the integration, assembly, augmentation as necessary, and testing of signal processing routines based on the various theoretical algorithms described above using the new instrumentation. Taken together, these items form the basis of a new long and intermediate wavelength reconstruction technology that promises to be of significant value to the inspection industry. Although the work is not finished, it is fair to say that first phase project goals have been exceeded, that certain problems have been defined, and that new options that follow from this work have been brought into focus.

ENGINEERING DEVELOPMENTS

Multiviewing Transducer System

Based upon initial simulation demonstrations in which it was experimentally shown that the size, shape, and orientation of a flaw could be determined using a multiviewing approach, a first generation composite transducer system has been designed, fabricated, and assembled. In this design, intended for water immersion use, six individual transducers are arranged in a hexagon about a central individual transducer. Each of the six peripheral transducers is placed in a gimbeled mount so that the angle of incidence (defined as the angle between the normal to the sample surface and the axis of the transducer) may be varied from 0° to 30°. The six transducers are then coupled to one drive system so that all six transducers can be set to the same angle (±1/4°) simultaneously. The angle is chosen so that the beams from all six peripheral transducers as well as the beam from the seventh center transducer intersect along the axis of the center transducer at any depth in the sample material. Additionally, each of the six peripheral transducers can be adjusted along its own axis at any angle setting by a second automating feature. The purpose of this automatic adjustment is to provide a means whereby the total elapsed time of beam propagation from ultrasonic pulse initiation to receipt of scattering signal is the same regardless of whether it is a pulse-echo pattern employing any one of the seven transducers or a pitch-catch pattern that requires any pair of transducers (center transducer and any one of the six peripheral transducers). Small digitally controlled motors are used to adjust both the angle of incidence and the propagation path distance. Figure 1 shows the multiprobe transducer at different stages of assembly. Since different individual transducers can be inserted into the assembly, the capabilities of the multiviewing probe can be tailored to inspection requirements by altering or mixing individual probe frequencies and beam patterns.

Electronic Circuitry

Electronic circuits have been assembled to activate the multiprobe using commercially available components wherever possible. The principal ultrasonic signal path of the system consists of the generation of an electronic voltage pulse in a Panametrics pulser and transmittal of the initiating pulse to the selected transducer through a Tektronix switch (MI5010) which is under control of a graphics computer that provides transducer selection and sequencing. The detected signal is transmitted back to the Panametrics receiver through a preamplifier of 20dB gain (Comlinear) that is protected from the initiating pulse by appropriate diode buffers and through the Tektronix switch. Each transducer of the assembly is coupled to a preamplifier. Detected wave forms are then transmitted to a Tektronix 7912AD converter where they are digitized, averaged, and stored in the graphics computer. Detailed calculations are then performed in the LSI 11/23 as they are needed. The graphics computer also serves as the control center to program and execute the inspection cycle. This portion of the cycle is done through a GPIB bus to the Tektronix switch and to the stepping motor drives that control the angle of incidence and transducer propagation path length. It is initiated through software programs for data acquisition that are described in the next section.

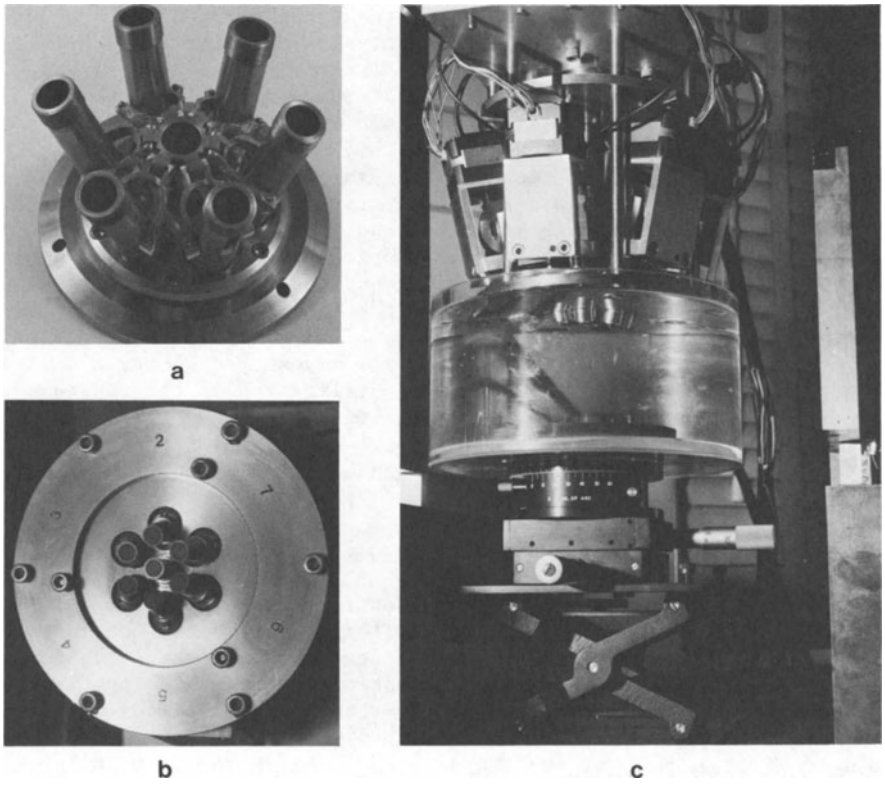

Fig. 1. Views of the multiviewing transducer.

a. base plate with gimbel transducer mounts
b. underside of base plate showing transducer cluster
c. assembled multiviewing transducer.

Data Acquisition

The data acquisition program that provides for automatic sequencing of the composite transducer and the acquisition of independent data records is quite detailed and performs very well. The velocity of sound in the host material inspected as well as other fixed constants of the composite transducer inspection geometry are required as input parameters. After a flaw signal is found utilizing the central transducer probe in a pulse-echo operation, the algorithm provides automatically for measurements to be made of other key set-up parameters that include the length of water path between the central transducer and the front surface of the sample and the depth of the flaw within the sample. These measurements are obtained by digitizing the elapsed time between the transmit pulse and the front surface reflection and flaw reflection, respectively. With this information, the required angle of incidence for the side-looking transducers is computed and set. Following this step, the circuit switches to a pitch-catch mode that contains the central transducer in the transmit mode and sequentially each of the six peripheral transducers in a catch mode. For

each one of these multiplex conditions, the total elapsed propagation time from the initiating pulse in the central transducer to receipt of flaw signal in the receiving peripheral transducer is digitized and compared with the previously measured roung trip pulse echo signal on the central transducer. Adjustments are then made automatically in the water path length for each of the side looking transducers so that the total transmit times are everywhere equal for all transmit-receive combinations. This equal timing feature has several advantages both in later data processing sequences and in the measurement of acoustic velocity differences in anisotropic media. Following these adjustments, the program automatically sequences the transducers through a combination of pulse echo and pitch catch combinations. At the present time, thirteen independent pieces of information are acquired. They consist of pulse echo responses on all seven transducers and six pitch catch responses resulting from utilization of the central and peripheral transducers. After acquisition, the wave forms are digitized and stored as described earlier. Additional independent as well as redundant records may be generated by changes in the control program.

Post-processing and Flaw Reconstruction

A first generation set of post-processing data procedures has been developed and implemented for use with the new multiprobe instrumentation. This set provides a 3-D reconstruction and characterization of volumetric flaws (size, shape, orientation and acoustic impedance estimates). The program can be run either automatically from beginning to end with no operator intervention or by individual segments selected from a menu. A summary of the steps in the program is given in Table I. This set of procedures represents the first step in the development of a structured decision-tree algorithm for flaw characterization.

Table I. Post-Processing and Reconstruction Algorithms

1.	Deconvolution, diffraction and attenuation corrections. (Measurement Model) (8)
2.	Flaw Size Estimation (1-D Inverse Born) (9)
3.	"Best-fit" Ellipsoid Regression Analysis. (Includes Front Surface Echo Analysis and size estimates from 2, and transformation to laboratory coordinates). (10)
4.	Display Options

Some comment should be made about item 3 in Table I. It is assumed in initiating the regression analysis that a general ellipsoid can be selected to "best fit" the data. The regression analysis then proceeds to determine values for the three semiaxes of the ellipsoid that determine its size and shape and three Euler angles that describe its orientation. The use of this technique was suggested by Kohn and Rice (11) as a way to approach the inverse problem in the long wavelength approximation. It is quite general and permits descriptions of either cracks (2D) or inclusions and voids (3D) to be obtained.

For example, a 2D element is closely approximated by a determination of three semi-axes if one of the semi-axes is small compared with the other two. Results from fracture mechanics show that failure initiating microcracks nucleate selectively about inclusions of various compositions and eventually grow into cracks under flaw growth conditions. While this assumption does not focus attention on the failure initiating microcracks per se, it does permit reasonable descriptions of the inclusions (or voids) that are necessary to nucleate the microcracking to be obtained. The use of the front surface echo analysis, which yields values of the acoustic impedance of the scatterer, assists in this matter. This measurement permits an estimate of the identity of the scattering center to be made (e.g., void, composition of inclusion) from which it can be predicted from material's knowledge whether or not there are likely to be surrounding microcracks. Theoretical advances in inverse scattering or the development of a prior history that describes specific characteristics of flaws in a given materials useage or processing environments may produce ways to eliminate the ellipsoidal assumption in the future, but until then, this assumption provides an adequate base for purposes of instrumental and signal processing development.

RESULTS

Examples of results obtained at various steps in the reconstruction process may be useful in understanding the processing steps (9). Figure 2a shows a stainless steel particle with the approximate shape of a prolate spheroid embedded in a Lucite host that was used for this reconstruction with semi-axes of 47 and 96 μm tilted about 7° from the parallel faces of the sample. In Fig. 2b is shown a polar plot of inversion results obtained at a variety of viewing angles. α' is the polar angle and β' is the azimuthal angle in the solid. The numbers given in the plot are values in μm of the tangent plane distances obtained from the inverse Born solution. Figure 2c shows the tangent plane distances of the equivalent ellipsoid obtained by the least squares iteration for both the x'z' and y'z' cross-section of the ellipsoid. Experimental points are also shown on the locus of tangent plane distances as circles (0). The experimental aperture is also readily apparent in this figure. The solid curve in Fig. 2d shows the final reconstruction of the best fit ellipsoid to the data. Points (0) shown are experimental points.

A summary of the various flaw characterization parameters and Euler angles obtained for the above example is given in Table II. In this summary, column A gives the derived sizing and orientation results using all 25 observation points within a conical half angle of 39°, column B gives results for 17 observation points within a conical half-angle of 26°, C shows the same results for 9 data points within a conical half-angle of 26°, and D shows results for only 6 data points - one at $\alpha'=0$, one at $\alpha'=19°$, and 4 at $\alpha'=11°$. It is evident that the density of data points used in D is too small to give good estimates of all six parameters (semi-axes and Euler angles), but that good results are obtained for the other cases. Oversizing on a_y, although not serious, is attributed to the "stub nosed" shape of the particle which departs substantially from a ellipsoidal shape. It should also be recalled that for small angles ($\theta \sim 7°$), equal and opposite values of ϕ and ψ correspond to compensating rotations about the z axis and together are essentially equal to 0.

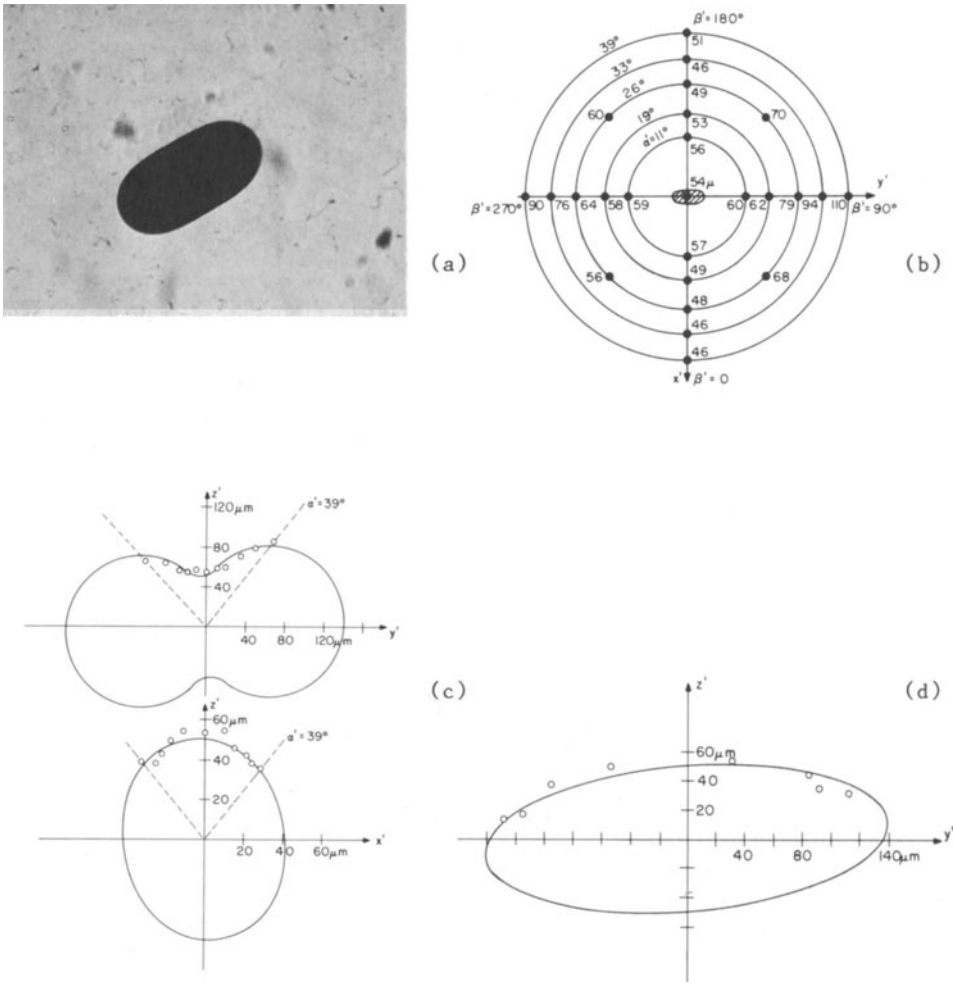

Fig. 2. Steps in the reconstruction process

a. 47x96μm steel sample in Lucite
b. sizing estimates at different polar and azimuthal angles
c. tangent plane distances at various interrogation angles
d. reconstructed "best fit" ellipsoid.

Other examples have also been examined with this new technique that include successful 3-D reconstructions of a void in titanium and an inclusion very near to a surface. The successful reconstruction of the latter is considered significant because of complications introduced in near-surface conditions (10,11).

Table II. Results of the ellipsoidal reconstruction for the 47x96μm (semi-axes) inclusions.

	Actual parameters	Ellipsoidal Reconstruction			
		A	B	C	D
a_x	47μm	40μm	27μm	28μm	0μm
a_y	96	141	119	123	122
a_z	47	50	54	53	56
θ	7°	14	8	9	2
ϕ	0	-71	-48	-47	7
ψ	0	69	47	46	8

First reconstruction results using the completely automated mode of the new instrumentation and signal processing algorithm have just been obtained. The sample used was a flat-surface diffusion bonded titanium sample that contains a machined oblate spheroidal void as a simulated defect with expected dimensions of 200 x 400μm (semiaxes). The z axis (symmetry axis 200μm) of the spheroidal shape is nominally normal to the sample's surface so that one Euler angle is expected to be 0° with the other two being indeterminate. This sample was specifically chosen for this first check-out of the automatic features of the new instrumentation for two reasons: 1) the sample had been utilized before in the earlier instrumental design studies so that earlier characterization data were available, and 2) the symmetrical features of the simulated defect permits an assessment of reproducibility and of the merits of redundant information and data point density to be made easily. Figure 3 shows one of the results of this automated experiment relating to the latter point. In this figure, derived sizes using the automated inverse Born are shown plotted against the estimated, or "true" size of the defect for both pulse echo and pitch catch combinations of the multiprobe array. The polar angles involved were 0° for the center pulse echo, 18° for the center-perimeter pitch-catch combinations, and 36° for the perimeter pulse echo points. For this particular simulated flaw, it is expected that the perimeter pulse echo values should all be the same and the center-perimeter pitch catch values should also be equal. With the exception of one "bad" point in the perimeter pulse echo values, it is evident that all values fall within ±25% of the expected value with the average being within ±5%. This result is considered very encouraging, for it involves a first test of several sequential steps each of which has been tested singly, but never before in an automatic sequencing mode. It is estimated that the "true" flaw size is the expected value ±15% with possible greater local deviations in the bonding plane.

In Table III the results of this first automated flaw characterization are compared with earlier results on this same sample using a simulated multiprobe transducer used for design purposes. (However, it is not known whether the results were obtained on the same side of the sample.) The first column in the table defines the parameters (semiaxes and Euler angles), the second gives expected values for these parameters, the third column gives results for the manual simulation experiment with 21 data points, and the last three columns give results for this

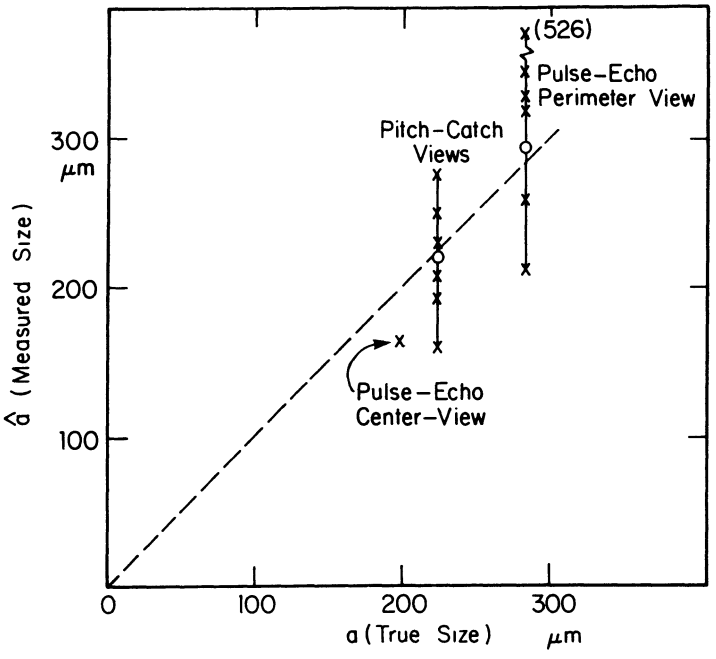

Fig. 3. Plot of measured sizes vs. true sizes for pulse echo and pitch-catch measurements.

Table III. Comparison of automatic and manual sizing measurements

Flaw Parameter	Expected Results	Manual Simulation	Automated Multiprobe WBDP	WOBDP	WADP
a_x	400μm	482μm	709μm	569μm	463μm
a_y	400	397	335	450	417
a_z	200	197	141	171	177
θ	0°	-2°	-6.9°	+3.2°	-5.7°
ϕ	----	----	----	----	----
ψ	----	----	----	----	----

first automated experiment. Results in column 4 were obtained using all 13 data points shown in Fig. 3 (with bad data point), column 5 gives regression analysis results without the bad data point (12 points), and the final column gives results in which the value of the bad data point in the fourth column apparently pushes the results out of bounds. Early results of a sensitivity analysis are given in another paper in this volume.

SUMMARY

Many advances have been made in the initial phase of this project toward the engineering development of a new, flaw characterization technology based on long and intermediate elastic wave scattering for quantitative ultrasonic NDE. These are summarized below.

- To the author's knowledge, the engineering prototype that has been assembled and automated represents the first instrumentation developed that will automatically provide a 3-D reconstruction of a flaw utilizing the long and intermediate elastic wave regimes. The configuration has been essentially prescribed by both theoretical advances in inverse scattering and laboratory feasibility experiments. Because of the automatic view-angle adjustment features, the multiprobe transducer can be utilized to look at flaws at any depth within a material.

- The signal processing package that has been assembled, augmented as necessary in this project, tested, and implemented has benefitted significantly from work done in other programs, principally the AF/DARPA work. There are a number of other inverse results, however, that remain to be woven together and evaluated as a part of the signal processing inventory. These include the long wavelength (11,12), probabilistic (5), and crack reconstruction algorithms (11,12). the signal processing package provides another unique feature. Since the model-based algorithms provide a way to define the center of the flaw and yield absolute flaw scattering amplitudes, information obtained is essentially independent of velocity anisotropies in the host medium.

ACKNOWLEDGEMENT

The Ames Laboratory is operated for the U.S. Department of Energy by Iowa State University under Contract No. W-7405-ENG-82. This work was supported by the Director of Energy Research, Office of Basic Energy Sciences.

REFERENCES

1. B. Budianski and J. Rice, J. Appl. Mech., 45, 453 (1978).
2. J. M. Richardson, Ultrasonics Symposium Proceedings (IEEE, New York, 1978), p. 759.
3. W. Kohn and J. R. Rice, J. Appl. Phys. 50, 3353 (1979).
4. J. H. Rose and J. A. Krumhansl, J. Appl. Phys. 50, 2951 (1979).
5. E. Domany, K. E. Newman, and S. Teitel, Proceedings of DARPA/AF Review of Progress in Quantitative NDE (AFWAL, 1979), p. 341.

6. J. M. Richardson and K. Fertig, Proceedings of DARPA/AF Review of Progress in Quantitative NDE (AFWAL, 1980), p. 528.
7. M. T. Resch, J. C. Shyne, G. S. Kino, and D. V. Nelson, in, Review of Progress in Quantitative NDE 1, D. O. Thompson and D. E. Chimenti, Eds. (Plenum Press, NY, 1982), p. 573.
8. R. B. Thompson and T. A. Gray, J. Acoust. Soc. Am. 74 (4), 1279 (1983).
9. D. K. Hsu, J. H. Rose and D. O. Thompson, J. Appl. Phys. 55 (1), 162 (1984).
10. D. O. Thompson and S. J. Wormley, in, Review of Progress in Quantitative NDE 3, D. O. Thompson and D. E. Chimenti, Eds. (Plenum Press, NY, 1984).
11. W. Kohn and J. R. Rice, J. App. Phys. 50, 3353 (1979).
12. J. D. Achenbach, K. Viswanathan, and A. N. Norris, Wave Motion 1, 299 (1979).
13. J. D. Achenbach, A. N. Norris, L. A. Ahlberg, and B. R. Tittmann, in, Review of Progress in Quantitative NDE 2, D. O. Thompson and D. E. Chimenti, Eds. (Plenum Press, NY, 1983), p. 1097.